Mine Water and the Environment (2018) 37:604–616
https://doi.org/10.1007/s10230-018-0510-8

TECHNICAL ARTICLE

Modeling the Effects of Phosphate Mining on Groundwater at Different Stages of Mine Development

Han Zhang[1] · Yu Wang[1] · Ruxing Yang[1] · Rongzhong Ye[2]

Received: 16 March 2017 / Accepted: 7 January 2018 / Published online: 20 January 2018

Abstract
In this study, a three-dimensional hydrogeological conceptual model was developed and a numerical model was calibrated with Visual MODFLOW to predict groundwater flow and evolution of groundwater field at different developmental stages at a large phosphate mine in Leibo, China, the Baku mine. ArcGIS was used to quantify changes in groundwater flow direction. The development of the cone of depression in the surrounding mining areas was predicted and the associated environmental impacts were discussed. At the beginning of mining, the cone of depression is limited to near each mining subarea and the drawdown is relatively small. The cone spreads out to the Liutong River as excavation proceeds. The model also estimated groundwater inflow rates into the different mining tunnels. The greatest inflow rate occurred in mining subarea M1.2 due to its large scale of mining and low elevation of the bottom of the tunnel. The results of this study can be used to plan optimal groundwater pumping and mine dewatering for safe mining at different mine development stages.

Keywords Groundwater flow · ArcGIS · Groundwater modeling · Water budget · Fractured rocks

Introduction

Lowering water tables prior to mining, i.e. dewatering, is done to maintain stable slopes and safe working conditions. However, aquifer dewatering poses considerable hydrological risks to regional groundwater by creating extensive and prolonged cones of depression, lowering the water table, and causing land subsidence and water deterioration (He et al. 2006). As mining continues, the risks increase, greatly threatening mine productivity and feasibility. It is therefore necessary to better understand how groundwater seeps into mines and predict groundwater level and groundwater discharge rates during the mining operation, and thus design a more effective dewatering procedure (Bahrami et al. 2014).

A number of methods have been developed and adopted to predict flows from surrounding strata and groundwater levels during various stages of mining. For example, analytical solutions have been used to estimate groundwater inflow into mines (Hanna et al. 1994; Singh and Atkins 1985). However, analytical solutions are based on assumptions and specific boundary conditions that limit their applicability in different mining situations. Numerical models can resolve some of the limitations of analytical solutions, especially when the aquifer is confined, fractured, and heterogeneous, and the flow is transient. Such models can provide a more realistic representation of interactions between groundwater systems and mining excavations when groundwater levels and the amounts of groundwater withdrawn are updated and calibrated/validated for every stage of mine development (Naidu et al. 2013; Rapantova et al. 2007). Numerical models have been successfully used to estimate groundwater inflows into karst aquifer systems (Rani and Chen 2010; Scanlon et al. 2003; Surinaidu et al. 2013b), coal mines (Younger and Harbourne 1995), and granitic aquifers (Surinaidu et al. 2013a). Some computer codes, such as MODFLOW and FEFLOW, have been widely used to predict groundwater inflow into mines and changes in groundwater level (Dafny et al. 2010; Sun et al. 2015; Surinaidu et al. 2014; Zhang 2013).

The objective of the present study was to estimate groundwater inflows into a mining tunnel at different stages of mining for optimal groundwater dewatering using a numerical groundwater model. This paper describes how

✉ Rongzhong Ye
zhanghan@home.swjtu.edu.cn

[1] Faculty of Geosciences and Environmental Engineering, Southwest Jiaotong University, Chengdu, China

[2] Department of Plant and Environmental Sciences, PeeDee Research and Education Center, Clemson University, Florence, SC, USA

the numerical flow model was used to resolve groundwater inflows into the mine during the different stages of mine development, and to assess the impact of mining on the regional groundwater system.

The Study Area

The Leibo region of Sichuan province is one of the most phosphate-rich areas in China. Total phosphate ore reserves in the area are estimated as 4.4 billion tons (BSGMRE 2012). The Baku mine is a large phosphate mine in the area, for which we developed a three-dimensional (3-D) hydrogeological conceptual model with Visual MODFLOW. The mine is divided into two parts (sections M1 and M2), with a total reserve of 6.7 million tons. The mine has a complex topography and structure and highly heterogeneous aquifers that present challenges to accurately simulating the groundwater flow field and groundwater discharges into the mine's tunnels.

The study area covers an area about 7.84 km^2 from 27°59′15″ to 28°03′00″ (N) and 103°21′15″ to 103°25′00″ (E). The elevation of the area ranges from 409 to 2000 m above sea level (m.a.s.l.), and it has a sub-tropical monsoon climate with a rainy season from May to September, followed by a cold, foggy winter up to February. Average annual rainfall (2001–2010) for the area varies from 635.5 mm to 1001.0 mm, with a mean of 828.3 mm. The mine is in the Jinshajiang basin, 6.23 km from the Jinshajiang River.

Geology

The geology of the study area was described by the Bureau of Sichuan Geology and Mineral Resources Exploration (BSGMRE 2012). The study area belongs to the Yangtze Paraplatform; its geology is summarized in Table 1 and Fig. 1.

The phosphate ore is mainly contained in the Maidiping Formation, which spans the depths of 125–200 m, and is divided into three layers. The top layer is characterized by a greyish white, medium-to-thick dolomite with phosphoric sand grains at the bottom. The middle layer is distinguished by greyish black, thin-to-medium economically valuable phosphorite rock strata with thin layers of phosphoric sand grains and dolomite. The bottom layer comprises phosphoric and silty dolomite with thin belts of phosphoric sand. There is a conformity between the bottom layers of the Maidiping and Dengying formations.

Hydrogeology

According to the lithology, stratigraphy, and structure of the geological strata, the water-bearing systems are delineated into minor, moderate, and major aquifers in the study area (BSGMRE 2012). The hydrogeological map and cross-section of the study area are presented in Figs. 2 and 3, respectively.

The lower Qiongzhusi and lower Canglangpu formations, which consist of siltstone and silty claystone, contain minor aquifers. The other minor aquifers are Quaternary sands and gravels in the sides of the valley and in low areas, and are not regionally significant. Moderate aquifers in the area are in the upper Qiongzhusi, upper Canglangpu, Maidiping, and Longwangmiao formations, which are composed of dolomitic limestone, limestone with inter-bedded siltstone, and claystone. The upper Qiongzhusi aquifer is distributed in both limbs of the Shaabo syncline and Liutong river anticline, with an outcrop area of 1.18 km^2 and a thickness of 35–70 m. The upper Canglangpu aquifer lies in both limbs of the Shaabo syncline and the west limb of the Liutong river anticline, with an outcrop area of 3.18 km^2 and a thickness of 50–80 m. The Longwangmiao aquifer lies in the core portion of the Shaabo syncline and the south boundary of the mine site, with an outcrop area of 1.14 km^2 and a thickness of 100–185 m.

The most important aquifers affecting mining activities in the study area exist in the Maidiping and Dengying Formations, which consist of dolomites and dolomitic limestone. The Maidiping major aquifer lies in the Shaabo syncline and both limbs of the Liutong River anticline, with a thickness of 30–243 m and an outcrop area of 6.37 km^2. The Dengying major aquifer is located east and southeast of the mine site, with a thickness of 400 m and an outcrop area of 8.72 km^2. The dominant recharge source of the aquifers is direct rainfall infiltration through permeable outcrops. Groundwater levels range from 759 to 2029 m.a.s.l., based on measurements in 50 boreholes drilled in the area. Transient groundwater levels in boreholes were also measured during 2010–2011.

Three faults, F1, F2, and F3 (Fig. 2), cut through the mineral deposit. Groundwater flows into the ore body through these faults due to their relatively high conductivities. The flow rate crossing the faults ranged from 1.63 to 11.01 L/s where mine tunnels penetrate the faults. These faults significantly affect mine operations and safety.

Groundwater Flow Modeling

Aquifer Conceptualization and Discretization

A 3-D visualization of the groundwater flow model was established with Visual MODFLOW, based on the

Table 1 Geological succession and hydrogeological properties of the study area

Erathem	System	Formation	Unit	Code	Thickness (m)	Lithology	Hydrogeological properties
Cenozoic	Quaternary			Q	0–20	Clay, sand and rocks	Minor aquifer
	Siluric	Longmaxi		S_1l	137–388	Shale with lamilated siltstone	Relative aquiclude
	Ordovician	Ungrouped		O^{2+3}	166–219	Limestone in the upside and sand shale in the bottom	Medium aquifer
	Cambrian	Erdaoshui		$\in_{3e}$	150–327	Primarily dolomitic limestone with shale at the top	Major aquifer
		Xiwangmiao		$\in_{2x}$	100–152	Siltstone with silty clay and fine sandstone	Medium aquifer
		Longwangmiao		$\in_1 l$	100–158	Grey-to-dark grey thick dolomitic limestone and dolomite, brecciaous gypsum at top	Medium aquifer
		Canglangpu	Upper	$\in_1 c^2$	50–80	Grey-dark grey medium-to-thick limestone with siltstone and silty claystone	Medium aquifer
			Lower	$\in_1 c^1$	70–110	Purple-red medium-to-thick beds of siltstone with thin-to-medium lenses of dolomite	Minor aquifer
		Qiongzhusi	Upper	$\in_1 q^2$	35–70	Greyish-green thin-to-medium dolomite with inter-beded calcite	Medium aquifer
			Lower	$\in_1 q^1$	200–500	Greyish black thin-to-medium siltstone and silty claystone with belts of clayish limestone	Minor aquifer
		Maidiping	Upper	$\in 1\ m^1$	23–99	Grey-greyish white medium- to-thick beds of dolomite with sand, dolomitic limestone at top, phosphoric gravel-sized grains at bottom	Major aquifer
			Middle	$\in 1\ m^2$	1.15–5.3	Greyish-black thin-medium dolomitic phosphorite rock with thin bed of phosphoric dolomite	
			Lower	$\in 1\ m^3$	6–137.8	Phosphorous micrite, silty dolomite with thin belts of phosphoric sands	
Proterozoic	Sinian	Dengying		Z_{bd}	> 400	Dark greyish-gray thick bed of dolomite	Major aquifer

geological and hydrogeological formations discussed above. The entire area was divided into 93 columns and 100 rows with a grid spacing of 100 m × 100 m in the flow model. The total model area was 93 km^2 (10.0 km × 9.3 km).

Six conceptual layers of variable thickness were used to represent the pertinent hydrogeological units. The top elevation of each layer was spatially variable and corresponded to surface elevations, based on topographic contours developed using a digital elevation model (DEM) of the area. The study area contains multiple water-bearing layers with different yields and hydrogeological parameters. Data used to develop and calibrate the groundwater model are summarized in Table 2.

Boundary Conditions and Model Parameters

Boundary conditions are a key component of the conceptualization of a groundwater flow system (Reilly 2001). River boundary conditions was assigned to the Jingsha River and the perennial Liutong Stream on the northern and northeastern parts of the area, using river bed elevations and river stage data collected in 2008–2009. Stream boundary conditions was assigned to the Ashayige and Xinchang Streams on the east and west part of the area. The western and eastern boundaries of the model were defined as no-flow boundaries. The northern boundary of the model was assigned a specified pressure head. The southern boundary of the model was made a flow boundary. The bottom borders of the area are no-flow boundaries, due to the presence of impermeable rock strata. Areal recharge was specified as a flux boundary condition. Aquifer recharge was distributed in six zones with different topographical and geological structures, and values were assigned as the product of mean annual rainfall and corresponding recharge infiltration coefficient of each geological formation. The recharge infiltration coefficients were initially assigned based on BSGMRE (2012), and then adjusted during the calibration of the groundwater steady-state flow model (Table 3).

A series of pumping tests were conducted in major aquifers during 2009–2011 by the BMRE to determine hydraulic conductivity. The values for the upper, middle, and lower Maidiping formation ($\in 1$ m, $\in 1\ m^2$, and $\in 1\ m^3$) are shown in Table 4. Hydraulic conductivities were initially

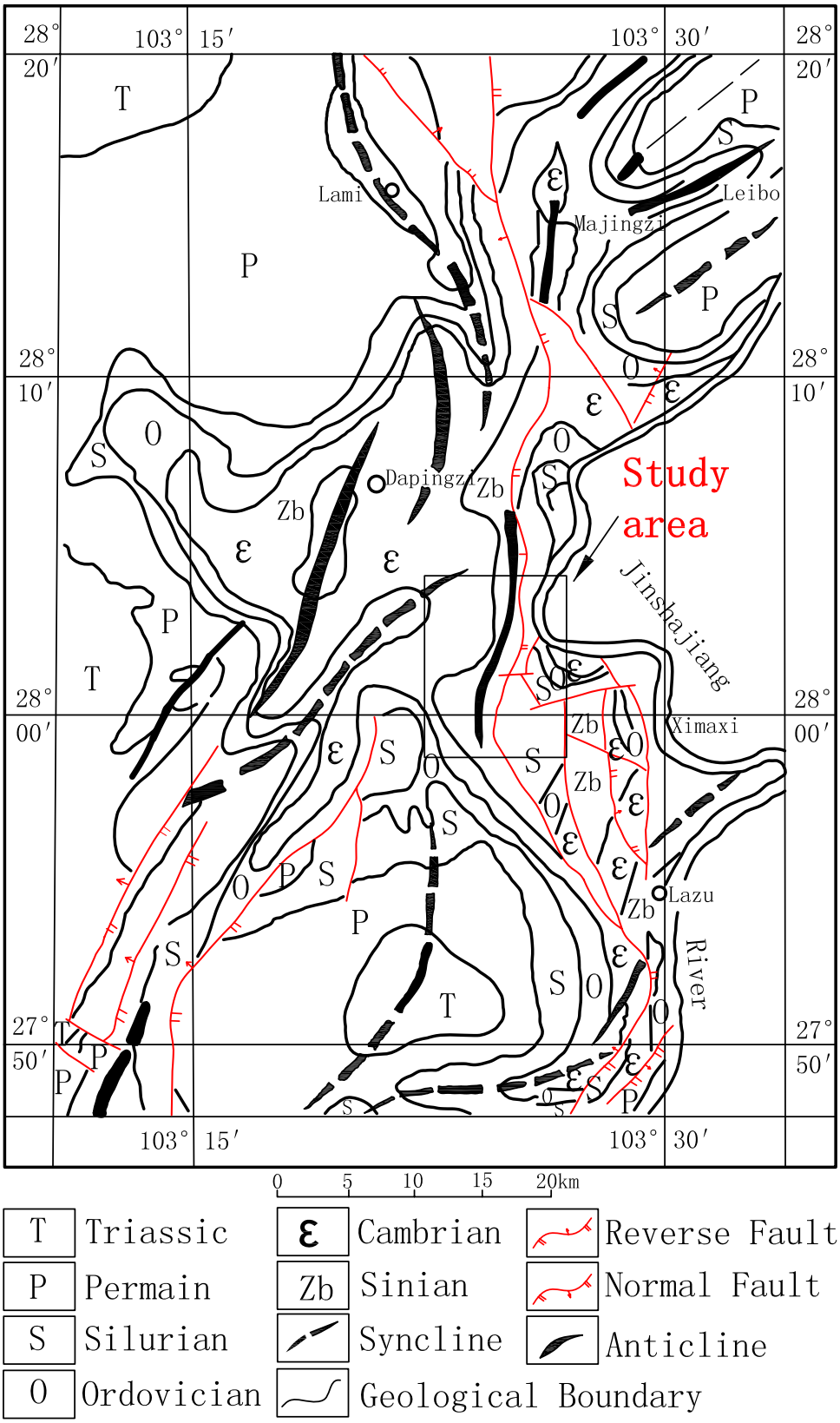

Fig. 1 Geological map of study area

assigned for the model's different formations i and modified during model calibration. Resultant horizontal hydraulic conductivities (x) are summarized in Table 4, while the horizontal y anisotropy and vertical z anisotropy were assigned

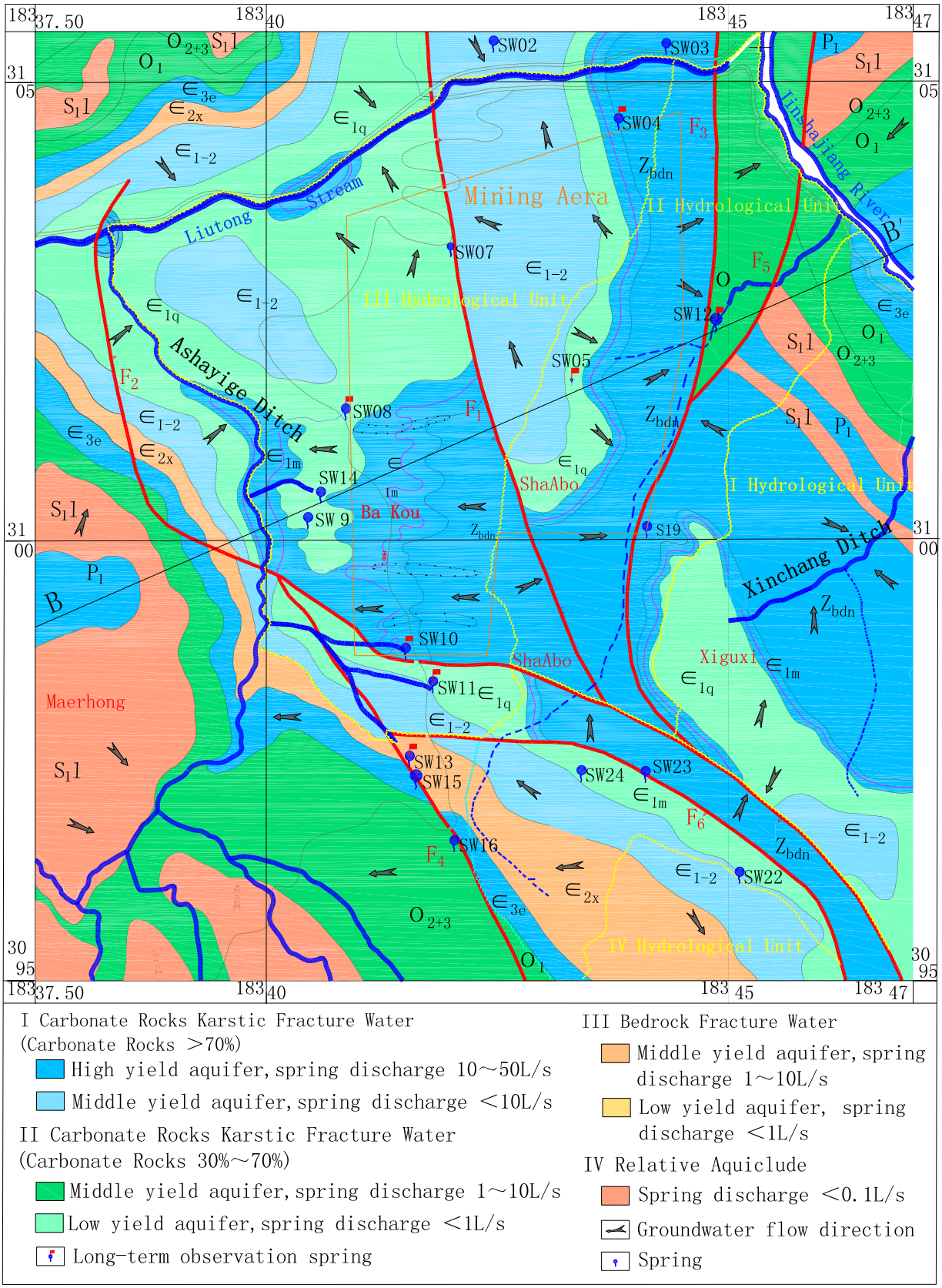

Fig. 2 Hydrogeological map of study area

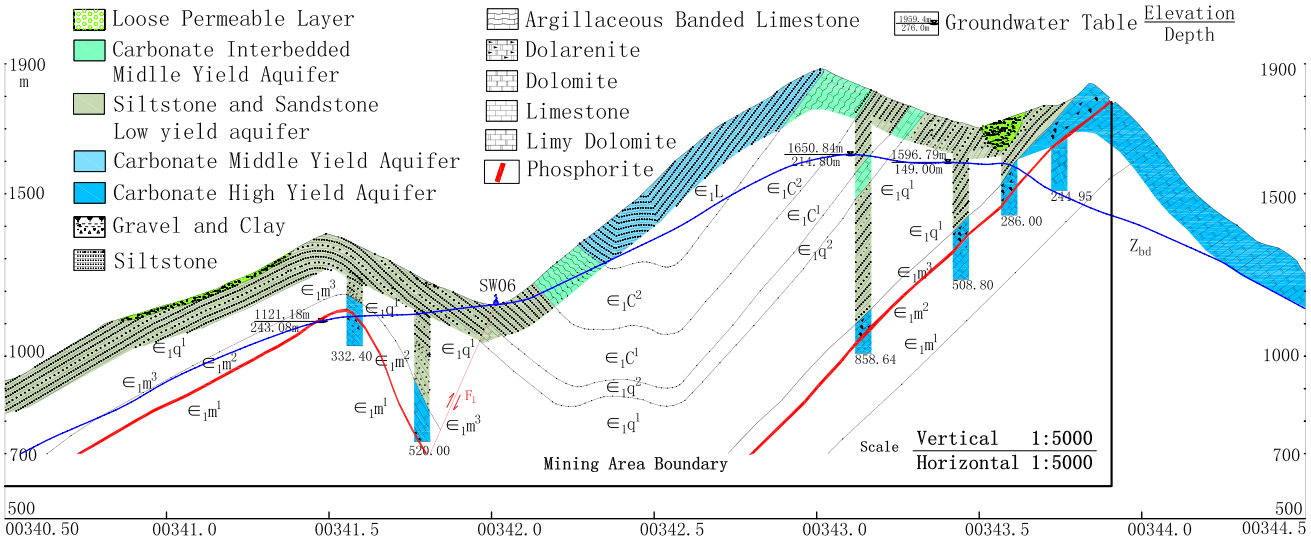

Fig. 3 B–B′ cross section of the study area

Table 2 Source, description and use of data in the groundwater model

Data	Source	Description	Use
Groundwater levels	Hydrogeology boreholes	Water level records in 2010 among 44 hydrogeology boreholes and two records per month (2010–2011) for two monitoring wells	Calibration of model and measured hydrographs
Flow and river heights	hydraulic geological report	Daily stream flow data and river heights from logs of three gauging stations	Defining the Liutong River, Jinsha River boundary conditions
Climate data	Hydraulic geological report	monthly precipitation and evapotranspiration data (2001–2010) from five weather stations	Calculation of recharge and flow boundary conditions into the model domain
Geology formation	Geology report	204 lithological logs and drillers' descriptions Bureau of Sichuan Geology and Mineral Resources Exploration	Aquifer conceptualization
Digital elevation model (DEM)	http://srtm.csi.cgiar.org	Arc-formatted ASCII and GeoTIFF	Elevation of the top layer of the groundwater model
GPS surveys of rivers	Field investigation	GPS surveys of river topography	River topography
Evaluation report of groundwater inflow	Hydraulic geological report	Dynamic observation record of mine hydraulic discharge	Suggestion of the volume of replaced pumping well
Hydrogeology conditions	Hydrogeology reports and map	plotting scale:1:25,000, Bureau of Sichuan Geology and Mineral Resources Exploration	Provide the basis for parameter division

values of 0.1 and 0.05, respectively. The hydraulic conductivity of the fault zones was 1.5 m/day (BSGMRE 2012).

Model Calibration

Model calibration is the process whereby model parameter structure and parameter values are adjusted and defined to provide the best match between measured and simulated groundwater levels and flows (Zheng and Bennett 2002). In this study, the groundwater flow model was calibrated to pre-mining groundwater levels measured in monitoring wells under both steady state and transient flow conditions.

Steady State Flow Model Calibration

Steady state flow model calibration was achieved through trial and error by adjusting two key parameters, hydraulic

Table 3 Recharge infiltration coefficient and other parameters in the model

Formations	Code	Hydraulic conductivity (m/day)	Specific storage (/m)	Recharge infiltration coefficient
Xiwangmiao formation	$\in_{2x}$	0.02	0.00005	0.15
Ungrouped formation	O_{2+3}	0.044	0.00008	0.26
Longwangmiao formation	$\in_{1-2}$	0.056	0.00008	0.26
Longmaxi formation	$S_1 1$	0.005	0.00001	0.1
Maidiping formation	$\in_{1m}$	0.076	0.0001	0.3
Qiongzhusi formation	$\in_{1q}$	0.01	0.00005	0.2

Table 4 Hydraulic conductivity estimated from pumping test

Borehole	Depth (m)	Surface elevation (m)	Groundwater depth (m)	Groundwater level (m)	Hydraulic conductivity (m/d)
ZK0602 $\in 1$ m[1]	384.14	1363.65	287.00	1076.65	0.021–0.068
ZK0603 $\in 1$ m[2]	445.85	1157.40	194.50	962.93	0.021–0.030
ZK1003 $\in 1$ m[2]	508.35	1747.20	125.10	1622.10	0.021–0.055
ZK1801 $\in 1$ m[3]	201.10	1982.70	195.50	1787.15	0.011–0.076
ZK1803 $\in 1$ m[3]	363.07	2008.40	136.70	1871.68	0.024–0.085

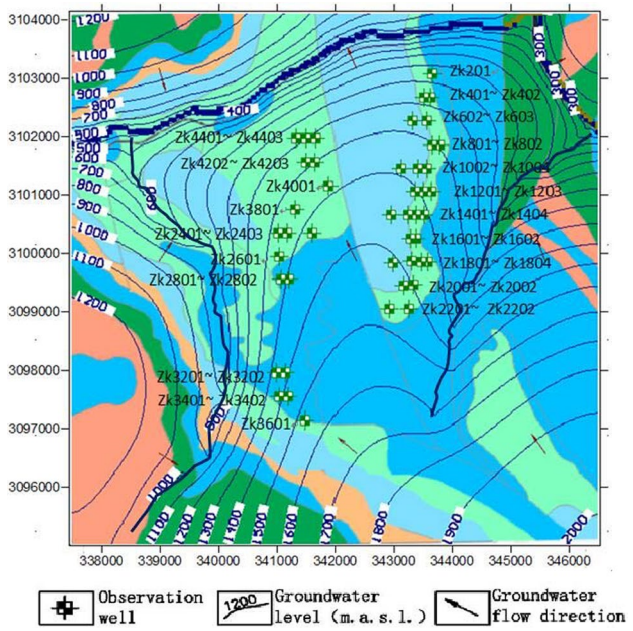

Fig. 4 Distribution of observation boreholes and groundwater levels (m.a.s.l.) simulated before mining

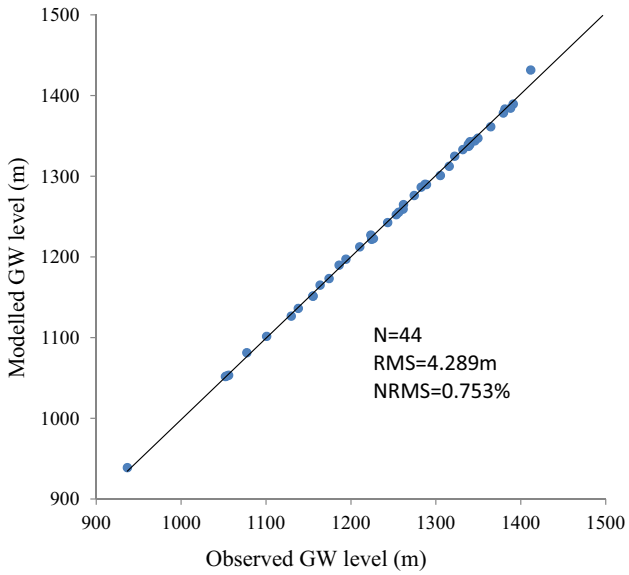

Fig. 5 Scatter plot of simulated versus observed values of groundwater level obtained in 44 observation boreholes in the steady state calibration

conductivity and recharge rate, using 44 observed groundwater levels measured in 2010 (Fig. 4). Model performance is shown in Fig. 5, with a root mean squared (RMS) error of 4.289 m and a normalized RMS error of 0.753%.

Since the trial-and-error calibration did not quantify the statistical uncertainty or reliability of the results, a sensitivity analysis was carried out to test the effect of uncertainty on the calibrated model. The analysis was based on the calibrated steady-state flow model, changing one parameter value at a time. The magnitude of the average change in groundwater head (e.g., RMS error) was used to describe the sensitivity of the solution to that particular parameter and condition. Hydraulic conductivity and recharge infiltration coefficient in the sensitivity analysis was varied linearly over a range from − 0.2 to + 0.2 (Table 5). It is apparent that the model was highly sensitive to both hydraulic conductivity and recharge.

Table 5 Results of sensitivity analysis of the steady-state flow model (expressed as RMS errors in groundwater level, m)

	− 20%	− 10%	− 5%	+5%	+10%	+20%
Hydraulic conductivity	106.97	50.03	18.53	15.92	25.81	63.86
Infiltration coefficient	73.69	30.68	13.01	12.42	23.42	60.99

Transient Calibration

To enhance simulation reliability, the model was also calibrated under transient state flow conditions. Simulated groundwater level values under transient state flow conditions depend on the aquifer's specific storage or yield and temporal distribution of recharge. As the aquifers in the study are confined aquifers, only specific storage was used. The initial specific storage values were based on BSGMRE (2012) and adjusted during the transient calibration (Table 3). The hydrographs of groundwater levels in two selected observation boreholes (zk1002 and zk2202) were used to assess the degree of fitness of the simulated and observed groundwater heads for 2010–2011. In general, the simulated values followed the patterns of the observed groundwater hydrographs (Fig. 6). The maximal RMS error was +2.25 m for zk1002 and −2.04 m for zk2202, respectively.

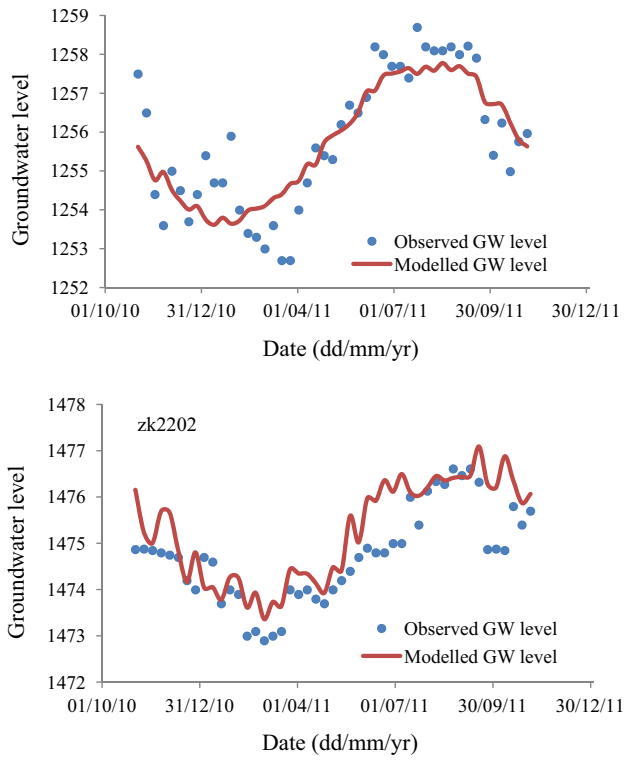

Fig. 6 Comparison between observed and simulated groundwater levels (m.a.s.l.) for the calibrated transient-state flow model

Results and Discussion

The calibrated groundwater flow model was capable of consistently integrating the measured data and conceptual model. It was then used to predict two practical interests related to groundwater in the Baku mining project: (1) environmental impacts on groundwater levels during mining, and (2) the risk of groundwater inflows and changes in water balance.

Mining Schedule

The Baku mining area is divided into two parts (M1 and M2) by a mountain ridge. Each part contains three subareas with different mining schedules (Fig. 7). The phosphate ore body is stratified and gently-inclined. A group of main mining tunnels and branch mining tunnels are constructed according to the shape of the ore body and its burial conditions. The tunnel intervals are 50 m in depth. Main mining tunnels are located on the elevation of 690, 1280, and 1370, m.a.s.l. for subareas M1.1, M1.2, and M1.3; 650, 1360, and 1450 m.a.s.l. for subareas M2.1, M2.2, and M2.3. During mining, groundwater inflow into branch mining tunnels is discharged into main mining tunnels, and then pumped out. The entire mining process consists of three stages: tunnel excavation, mining, and post-mining. The period of the predictive model is 25 years. The distribution of subareas and tunnels layout are shown in Fig. 8.

Prediction of Groundwater Flow Field

Groundwater inflow into a mine tunnel at different stages of mining was simulated with the "Well" package in Visual

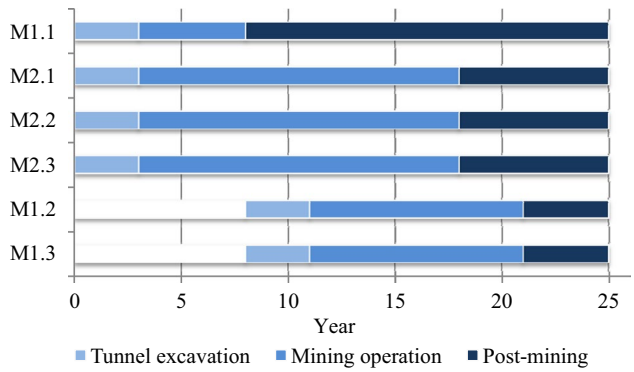

Fig. 7 Mining subareas and mining schedule

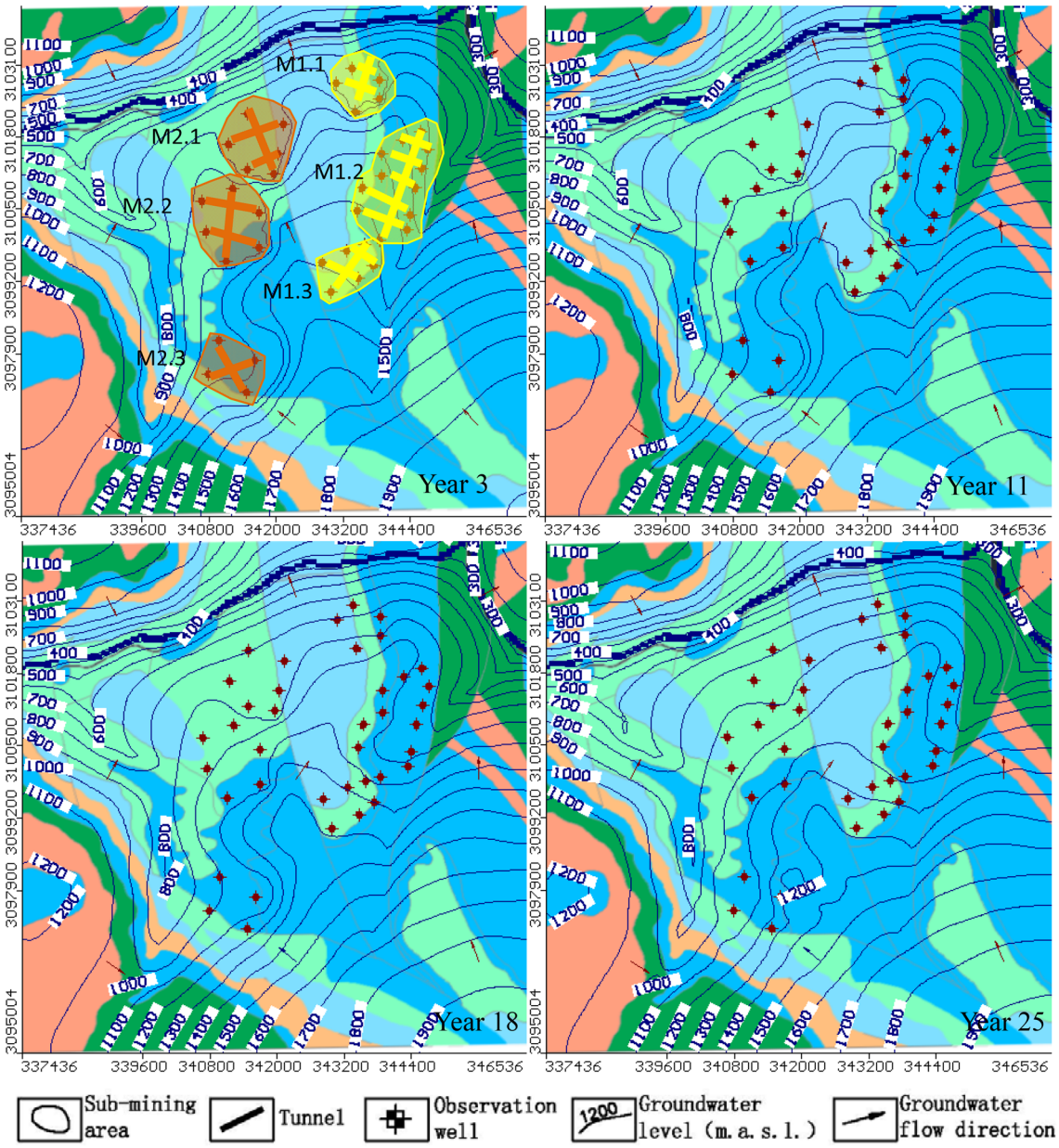

Fig. 8 Evolution of groundwater flow field during different mining stages

MODFLOW. Predictive simulations were performed in transient conditions. Pumping wells were turned on during tunnel excavation and shut off in the post-mining period in the model according to the schedule (Fig. 7). Groundwater inflow into the tunnel lowers the water table and pumping wells around a subarea decreases the water table progressively if pumpage exceeds the natural recharge to the system. A trial and error method was used to determine optimal pumping rates to manage the water levels in each well at the desired level, below the elevation of the tunnel bottom, at the end of the tunnel excavation period.

Figure 8 is a contour map of groundwater levels showing changes in the groundwater flow fields for the next 3, 11, 18, and 25 years. With continuous pumping from the wells, hydraulic gradients appeared, allowing aquifer groundwater to flow into the mine tunnels from all directions. It was assumed that pumping was shut off after mining and that groundwater levels in the impacted aquifer wells began to recover.

In addition, ArcGIS was used to quantify the changes in groundwater flow direction. Groundwater level data were treated as DEM data in Slope Analysis in ArcGIS. Assuming groundwater flows from higher levels to lower ones, the direction of groundwater flow changed as the hydrological

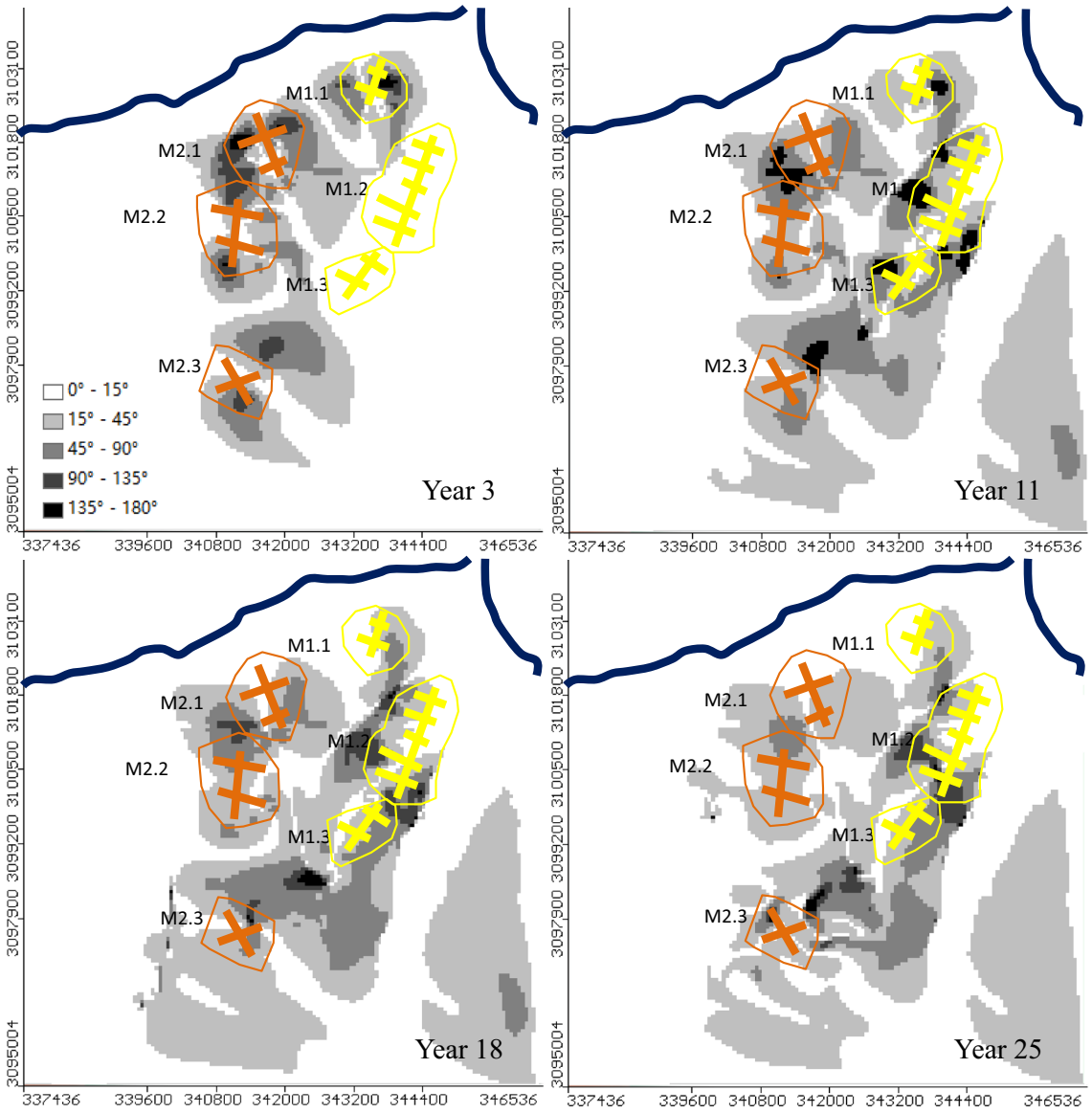

Fig. 9 Groundwater flow direction shifting areas during different mining stages

gradient changed. By comparing the groundwater flow in year 3, 11, 18, and 25 since the start of mining, a map was developed showing the areas with different degrees of changes in flow direction (Fig. 9). In Fig. 9, dark areas indicate the great shift of groundwater flow direction while light areas means small shifts of groundwater flow direction compared to the natural flow direction before mining.

Large changes in groundwater flow direction occurred mainly in the center of the study area, while small changes were found near the Liutong and Jingsha Rivers, indicating that the relationship between surface water and groundwater was not affected significantly by mining. Since the river surface is lower than the bottom of the tunnel, groundwater discharges to the rivers during the entire mining process.

Prediction of the Cone of Depression

The development of the cone of depression is shown in Fig. 10. At the beginning of mining, the cones of depression are limited to near the mining subareas, and the drawdown is relatively small. In year three, cones of depression occurs in subareas M1.1, M2.1, M2.2, and M2.3, in response to tunnel excavation. As more tunnels were excavated and pumping continued, the cone spread out to the Liutong River and formed a larger area of depression. Groundwater levels of the cone center in subareas M2.1 and M2.3 dropped 400, and 300 m in the other subareas. During mining, the cone of depression gradually expanded towards the south. Tunnel excavation and mining were supposed to end in year 21.

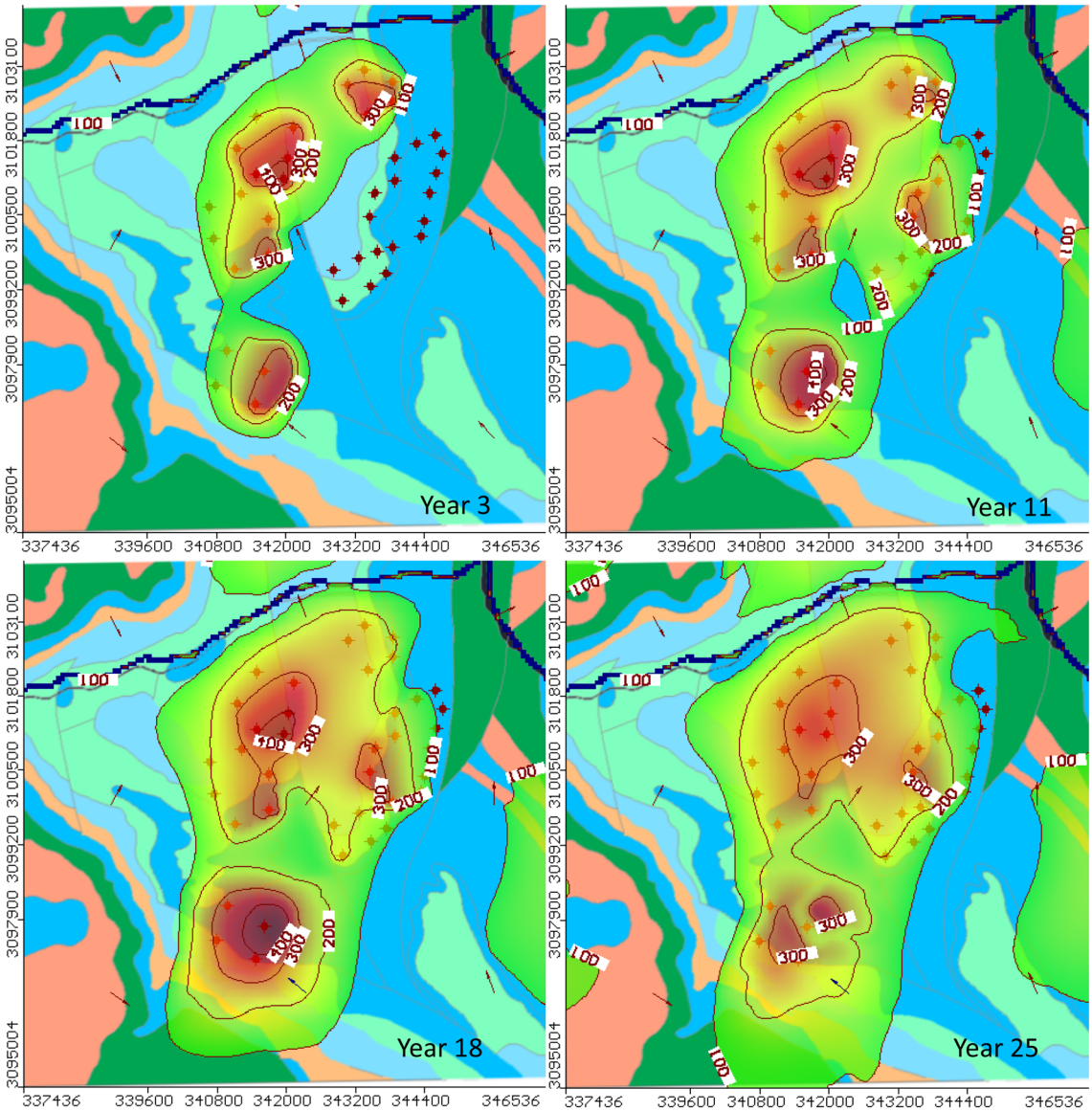

Fig. 10 Development of depression cone (m) during different mining stages

The edge of the cone of depression did not spread out to the model boundary during this period and therefore the model was considered to be appropriate for prediction. Since pumping wells were shut off during the post-mining period, the center of the cone of depression rose from year 22 and the effects of mining on the groundwater system were alleviated during years 22–25, although the edge of the cone continued to spread out to the southern boundary.

Groundwater Inflow Rate and Water Budget

The predicted rates of groundwater inflow to the subareas was estimated by summing the pumping rate in each corresponding subarea (Fig. 11). The groundwater inflow rate depends on the scale of mining and the difference in the elevation between the tunnel bottom and ambient groundwater. The greatest inflow occurred in subarea M1.2 due to its large mining scale and lower tunnel elevation; the rate of groundwater inflow was 11,686 m^3/day at the beginning of tunnel excavation (year 9) and dropped as low as 3062 m^3/day during mining (year 12), followed by a progressive decrease to 1622 m^3/day by the end of mining. Similar patterns were observed in the other mining areas, with relatively less flow.

Groundwater balance for subareas M1 and M2 at the three stages are summarized in Table 6. During tunnel excavation, groundwater discharge into the tunnel was a main output component of the aquifer: 17,050 and 38,175 m^3/day for M1 and M2, respectively. In this stage, significant groundwater,

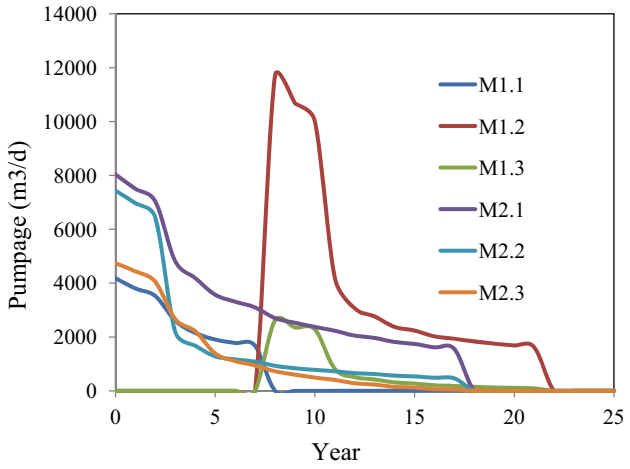

Fig. 11 Dynamic groundwater inflows into different mining subareas in the study area

Table 6 Groundwater balance in the study area

Input in m^3/day		Output in m^3/day	
Mining part M1 during tunnel excavation			
Lateral inflow	4489	Lateral outflow	− 508
Recharge	1818	Mining tunnel	− 17,050
Storage	11,280	River and ditch	− 30
Mining part M1 during mining operation			
Lateral inflow	2503	Lateral outflow	− 469
Recharge	1912	Mining tunnel	− 4892
Storage	975	River and ditch	− 28
Mining part M1 during post-mining			
Lateral inflow	847	Lateral outflow	− 470
Recharge	1278	Mining tunnel	0
Storage	− 1628	River and ditch	− 27
Mining part M2 during tunnel excavation			
Lateral inflow	6914	Lateral outflow	− 1975
Recharge	1434	Mining tunnel	− 38,175
Storage	31,954	River and ditch	− 152
Mining part M2 during mining operation			
Lateral inflow	2048	Lateral outflow	− 380
Recharge	1433	Mining tunnel	− 4644
Storage	1572	River and ditch	− 30
Mining part M2 during post-mining			
Lateral inflow	824	Lateral outflow	− 494
Recharge	1434	Mining tunnel	0
Storage	− 1727	River and ditch	− 36

11,280 and 31,954 m^3/day for M1 and M2 were removed from aquifer storage, resulting in continued groundwater level declines. During mining, discharge into the tunnels was still a major outflow component of the aquifer although water drawn from storage declined. After mining, no water discharged to the tunnel and recharge refilled the aquifer storage. During all three stages, groundwater discharged to the river and ditch, which explains the unchanged flow direction of groundwater toward the Liutong and Jinsha Rivers. The decline in groundwater levels due to mining also affects springs. Some springs in the south are expected to go dry during and after mining; therefore, alternative water supply sources should be provided for local use.

Conclusions

The present study used an equivalent porous media approach to simulate the complex processes of groundwater flow in a fractured dolomitic limestone groundwater system. A 3D hydrogeological conceptual model was developed with Visual MODFLOW to simulate long-term groundwater inflows into the mine tunnels. Sensitivity analysis demonstrated that the simulated results are highly sensitive to the hydraulic conductivity and recharge infiltration coefficient. Groundwater inflow into the mining areas mainly depended on mining scale and the relative levels of the bottom of the tunnels and surrounding groundwater. Subarea M1.2 will experience a maximum groundwater inflow of 11,686 m^3/day into the tunnel at the beginning of tunnel excavation. The computed groundwater budget indicated that, during tunnel excavation, the inflowing water (11,280 and 31,954 m^3/day for M1 and M2, respectively) was mainly from aquifer storage, though lateral inflow and natural recharge also contributed. There will be less inflow during mining than during tunnel excavation.

This study represents a significant advance in understanding groundwater flows in the region and the results can be used to design an effective groundwater management program to reduce environmental risks and fatalities. Better quantifications of hydrogeological characters of the landscape will minimize modeling uncertainties and thereby improve the designed management outcomes.

Acknowledgements This study was supported by the China National Science Foundation (Grant 51509215) and the Chengdu Science and Technology Bureau Foundation (Grant 2015-HM01-00350).

References

Bahrami S, Doulati AF, Aslani S, Baafi E (2014) Numerical modelling of the groundwater inflow to an advancing open pit mine: Kolahdarvazeh pit, central Iran. Environ Monit Assess 186:8573–8585. https://doi.org/10.1007/s10661-014-4025-x

BSGMRE (2012) Report of geology survey on the Baku phosphorous mine in Leibo County, Sichuan Province. Bureau of Sichuan Geology and Mineral Resources Exploration, Chengdu **(in Chinese)**

Dafny E, Burg A, Gvirtzman H (2010) Effects of karst and geological structure on groundwater flow: the case of Yarqon-Taninim Aquifer, Israel. J Hydrol 389:260–275

Hanna TM, Azrag EA, Atkinson LC (1994) Use of an analytical solution for preliminary estimates of groundwater inflow to a pit. Min Eng 46:149–152

He KQ, Guo D, Wang XW (2006) Mechanism of the water invasion of Gaoyang Iron Mine, China and its impacts on the mine groundwater environment. Environ Geol 49:1163–1172

Naidu LS, Rao GV, Rao T, Mahesh J, Padalu G, Sarma VS, Prasad PR, Rao SM, Rao BM (2013) An integrated approach to investigate saline water intrusion and to identify the salinity sources in the central Godavari delta, Andhra Pradesh, India. Arab J Geosci 6:3709–3724

Rani FM, Chen ZH (2010) Numerical modeling of groundwater flow in karst aquifer, Makeng mining area. Am J Environ Sci 6:78–82

Rapantova N, Grmela A, Vojtek D, Halir J, Michalek B (2007) Ground water flow modeling applications in mining hydrogeology. Mine Water Environ 26:264–270

Reilly ET (2001) System and boundary conceptualization in groundwater flow simulation. U.S. Geological Survey, Branch of Information Services

Scanlon RB, Mace ER, Barrett EM, Smith B (2003) Can we simulate regional groundwater flow in a karst system using equivalent porous media models? Case study Barton Springs Edwards Aquifer, USA. J Hydrol 276:137–158

Singh RN, Atkins AS (1985) Application of idealised analytical techniques for prediction of mine water inflow. Min Sci Technol 2:131–138

Sun WJ, Wu Q, Liu HL, Jiao J (2015) Prediction and assessment of the disturbances of the coal mining in Kailuan to karst groundwater system. Phys Chem Earth 89–90:136–144

Surinaidu L, Bacon CGD, Pavelic P (2013a) Agricultural groundwater management in the Upper Bhima Basin, India: current status and future scenarios. Hydrol Earth Syst Sci 17:507–517

Surinaidu L, Gurunadha Rao VVS, Ramesh G (2013b) Assessment of groundwater inflows into Kuteshwar Limestone Mines through flow modeling study, Madhya Pradesh, India. Arab J Geosci 6:1153–1161

Surinaidu L, Gurunadha Rao VVS, Srinivasa Rao N, Srinu S (2014) Hydrogeological and groundwater modeling studies to estimate the groundwater inflows into the coal mines at different mine development stages using MODFLOW, Andhra Pradesh, India. Water Resour Ind 7–8:49–65

Younger PL, Harbourne HJ (1995) To pump or not pump: cost benefit analysis of future environmental management options for the abandoned Durham coalfields. Water Environ J 9:405–415

Zhang GW (2013) Type curve and numerical solutions for estimation of transmissivity and storage coefficient with variable discharge condition. J Hydrol 476:345–351

Zheng C, Bennett GD (2002) Applied contaminant transport modeling, 2nd edn. Wiley, New York